Journal of Materials Chemistry C

PAPER

View Article Online
View Journal | View Issue

Cite this: J. Mater. Chem. C, 2019, 7, 11639

Rational molecular design for isoindigo-based polymer semiconductors with high ductility and high electrical performance†

Fengshou Tian,[a] Han Chen,[a] Yuchang Du,[ab] Junhui Chen,[a] Xiaohong Wang,*[a] Hongbo Lu,[a] Kilwon Cho,[c] Guobing Zhang[a] and Longzhen Qiu*[ab]

Achieving good electrical properties and ductility of polymer semiconductors has always been challenging. In this work, a series of isoindigo derivative-based conjugated polymers was studied in an effort to gain a better understanding of the influence of polymer main and side chain structures on their electrical and mechanical properties. The results suggested that the introduction of alkyl side chains onto the donors can significantly enhance the mechanical properties of isoindigo-based polymers; however, the electrical properties of the films greatly deteriorated due to the large steric hindrance by the chain. The insertion of strong electron-withdrawing units, such as benzodifurandione, into the isoindigo chain during the synthesis of a bis(2-oxoindolin-3-ylidene)-benzodifuran-dione (BIBDF)-based polymer (PBIBDF-BT) significantly boosted the electrical properties of the films without decreasing their mechanical properties. The crack onset in PBIBDF-BT thin films was observed at 50% tensile strain. In addition, PBIBDF-BT thin films exhibited bipolar transport properties with both electron and hole mobilities greater than 0.1 $cm^2 V^{-1} s^{-1}$ at 100% strain. It is found that the improvement of PBIBDF-BT performance is attributed to its proper molecular structure. The long alkyl side chains significantly increase the ductility of PBIBDF-BT thin films, and the strong electron-withdrawing BIBDF unit in the main chains enhances the local aggregation, resulting in a significant increase in mobility. These results indicate that the mechanical and electrical properties of conjugated polymers could simultaneously be improved through reasonable molecular design.

Received 18th June 2019,
Accepted 23rd August 2019

DOI: 10.1039/c9tc03263k

rsc.li/materials-c

1. Introduction

Polymer semiconductor materials have been widely used in flexible electronics due to their inherent advantages, such as high mechanical flexibility and solution processability.[1–5] Though polymer semiconductors based on carbon frames have a certain degree of flexibility, their rigid π-conjugated backbone and highly ordered aggregate structures (required for effective charge transfer) often yield hard and brittle mechanical properties, rather than the strong and tough characteristics similar to engineering plastics or rubber.[6–8] Therefore, the development of ductile semiconductors for wearable and implantable plastic electronic devices remains challenging.[9,10]

In the past few years, numerous studies have been carried out to explore the relationship between mechanical properties and structures of conjugated polymers. Some methods led to improvements in the mechanical properties of polymers. One approach consisted of introducing soft amorphous moieties into conjugated polymer films either by physic blending or by chemical modification.[11–13] For suitably designed polymer films containing crystalline and amorphous regions, the applied stress would preferentially dissipate in the relatively soft amorphous region.[14] Previously, we synthesized semiconducting tri-block copolymers of poly(3-hexylthiophene)-*block*-poly(methyl acrylate)-*block*-poly(3-hexylthiophene) and noticed that they behave like thermoplastic elastomers with an elongation at break of 140% and modulus of 6 MPa.[15] Cho *et al.* blended poly(3-hexylthiophene) (P3HT) nanowires (NWs) with poly(dimethylsiloxane) (PDMS) to yield P3HT NW networks embedded in PDMS matrix. Even at 50% strain, P3HT NW/PDMS blends retained continuous P3HT NW networks with few cracks and

[a] National Engineering Lab of Special Display Technology, State Key Lab of Advanced Display Technology, Academy of Opto-Electronic Technology, Hefei University of Technology, Hefei 230009, China. E-mail: xhwang11@hfut.edu.cn, lzhqiu@hfut.edu.cn
[b] Anhui Province Key Laboratory of Advanced Functional Materials and Devices, School of Chemistry and Chemical Engineering, Hefei University of Technology, Hefei 230009, China
[c] Department of Chemical Engineering, Pohang University of Science and Technology, Pohang 790-784, South Korea

† Electronic supplementary information (ESI) available. See DOI: 10.1039/c9tc03263k

low mobility around 10^{-3} cm^2 V^{-1} s^{-1}.[16] However, this route often introduces a large number of insulating polymers and reduces the carrier mobility. Moreover, chemical differences between polymers may lead to nano- or micro-scale phase separation and deterioration of device performance over time.[17]

Another method based on molecular modification of main and side chains has been found to improve the overall flexibility of polymer films without sacrificing charge transport.[18,19] The use of conjugated breakers, designed initially to improve solution processability of polymer semiconductors, might enhance stretchability by the addition of non-conjugated structural units to the main chain to break the conjugated structures.[20,21] Bao *et al.* utilized various length alkyl chains as conjugation breakers and recorded higher fracture strains reaching 130%.[22] The introduction of branched alkyl side chains or increase in length of side chains might reduce the tensile modulus and glass transition temperature, making conjugated polymer properties closer to "rubbery" at ambient temperature for better ductility.[3,14,23] Cross-linked films also displayed increased elastic modulus and increased fracture strain due to the plasticizing effect of soft siloxane cross-linkers.[24] Overall, the above provided examples look promising for the development of new semiconductor materials with good electrical properties and stretchability; however, the scheme and design mechanism for the semiconductor materials with good tensile and electrical properties are still limited, which still needs to be explored.[25,26]

Amide-containing dyes such as isoindigo have been extensively used as acceptor units for constructing high-performance donor–acceptor polymers because they have many advantages such as good coplanarity, strong electron-deficiency, and adjustable solubility.[27–30] Furthermore, isoindigo is easy to synthesize and has a strong modifiability. In recent years, chemists have systematically modified the isoindigo unit, and developed a series of novel derivatives and their conjugated polymers.[31–34] These results facilitated the study of the relationship between polymer structure and its electrical and mechanical properties. Based on the above considerations, a series of isoindigo-based conjugated polymers with different main and alkyl side chains was designed and prepared (Fig. 1a). The properties of polymers

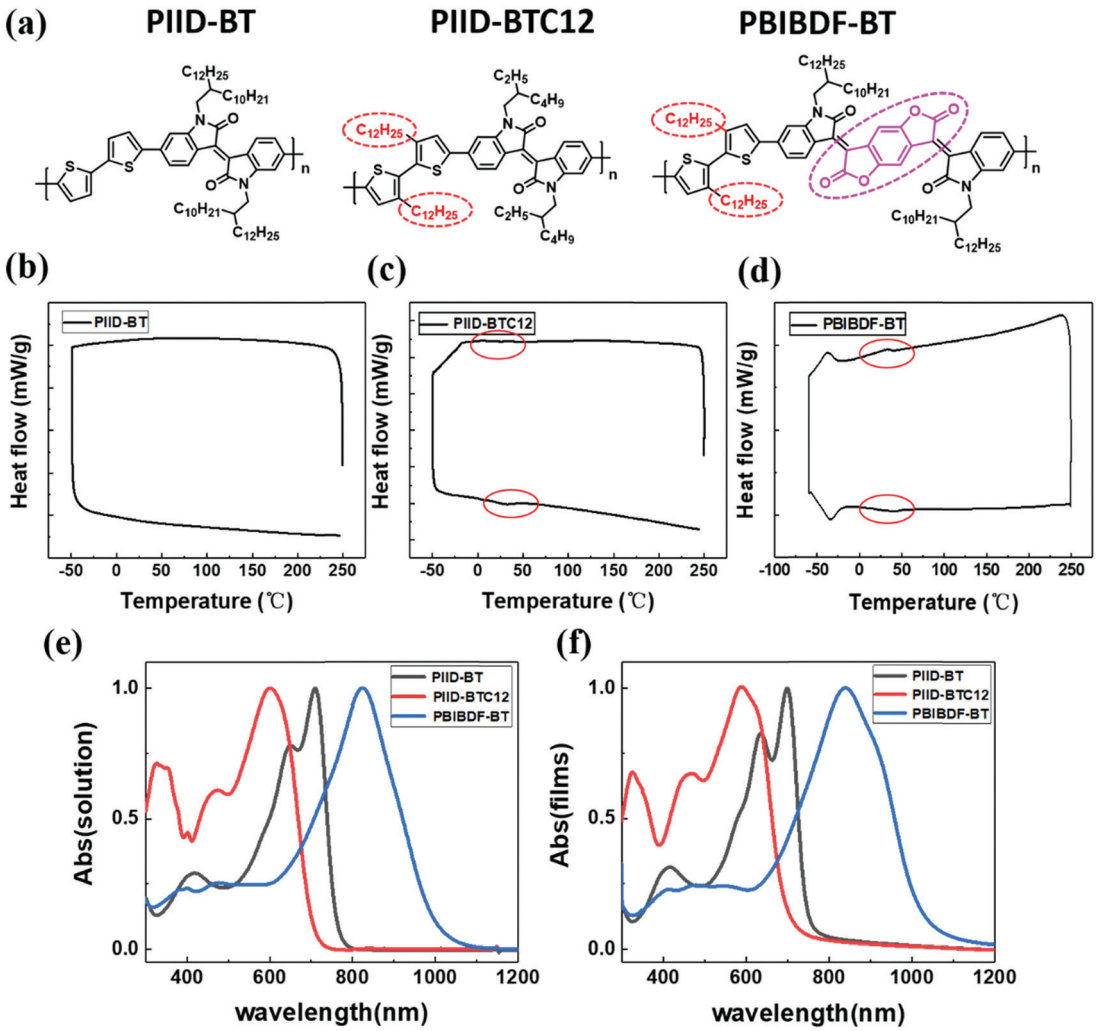

Fig. 1 (a) Chemical structures of isoindigo and its derivative-based polymers. (b–d) DSC thermograms of the three polymers at a heating/cooling rate of 20 °C min^{-1}. (e and f) Normalized UV-vis absorption spectra of PIID-BT, PIID-BTC12, and PBIBDF-BT in solution and in thin films.

were systematically regulated by modifying the polymers with side groups and strong electron-withdrawing groups, such as conjugation degree, planarity, energy level, molecular arrangement and crystallinity. It was found that these changes have significant effects on the field-effect properties and mechanical stretchability. Our research provided an effective strategy for the design of polymers with good electrical properties and mechanical flexibility.

2. Experimental

2.1 Materials

All the solvents were purchased from Sinopharm Chemical Reagent Co., Ltd and used as received. Polydimethylsiloxane (PDMS, Sylgard 184, Dow Corning) was mixed at a weight ratio of 10 : 1 and then cured at 80 °C for 10 hours. Octadecyltrichlorosilane (OTS) was purchased from Sigma-Aldrich Chemical Ltd. All polymer semiconductor materials were synthesized by our group (Fig. S1 of the ESI†).

2.2 Preparation of the semiconductor layer

Highly doped Si wafers were cut into 1.5 × 1.5 cm^2 pieces. The wafers were cleaned with a mixture of concentrated sulfuric acid and hydrogen peroxide solution (7 : 3, v/v) for 90 minutes. Then, the cleaned wafers were modified with OTS self-assembled monolayer.[35] Polymer solutions with the same concentration (6 mg ml^{-1}) were spin-coated on OTS-modified Si substrates. The thickness of the obtained polymer thin films was 35 ± 2 nm.

2.3 Preparation of stretched thin films and the OFET device

The film-on-elastomer method was used to prepare the stretched thin films.[36] First, the thin films were laminated with PDMS substrate and peeled off from the OTS-treated Si substrate, stretched at a certain ratio and then transferred to a second silicon wafer for optical microscope testing and atomic force microscope testing. For measuring the electrical performance of the stretched polymer thin films, the PDMS/semiconductor bilayers were stretched to a certain strain and then the films were transferred to Si substrates with 300 nm SiO_2 layers. The bottom-gate/top-contact device structure was defined by 100 nm thick Au through regular shadow masks, and the channel length (L) and width (W) were 100 and 1000 μm, respectively.

2.4 Characterization

The optical UV behavior of these polymer thin films was recorded on a PerkinElmer model λ 20 UV-vis spectrophotometer. The morphologies of the transferred thin films were characterized *via* atomic force microscopy (AFM) in tapping mode (Digital Instruments Multimode). Electrical characterization of stretched thin films was performed using a Keithley 4200-SCS semiconductor parametric analyzer. Grazing incidence X-ray diffraction was performed at the Pohang Accelerator Laboratory (PAL) in Korea.

3. Results and discussion

Polymer characterization

The polymers of PIID-BT and PBIBDF-BT were synthesized following the method reported by previous literature.[31–34] PIID-BTC12 was synthesized through a similar Stiller coupling reaction route (Fig. S1, ESI†). The detailed synthetic procedures and characterization of the three polymers are shown in the ESI.† PIID-BT, PIID-BTC12 and PBIBDF-BT showed number-averaged molecular weights of 37.1 kDa (PDI = 3.35), 35.0 kDa (PDI = 2.67) and 42.4 kDa (PDI = 1.89), respectively. Thermogravimetric analysis suggested that all three polymers had reliable thermal stabilities, with 5% weight loss at a thermal decomposition temperature of 350 °C (Fig. S2, ESI†). This temperature would guarantee high-temperature device processing based on these polymer thin films.

The thermal properties of the three bulk polymers were evaluated *via* differential scanning calorimetry (DSC) at continuous heating and cooling rates (Fig. 1b–d). Consistent with previous literature, PIID-BT (Fig. 1b) did not exhibit obvious melting or a crystalline thermal transition and glass transition within the measured temperature range, indicating a rigid backbone with resistance to thermal disturbances. PIID-BTC12 (Fig. 1c) and PBIBDF-BT (Fig. 1d) depicted endothermic transitions at about 38 and 46 °C, and exothermic transitions at around 24 and 37 °C, corresponding to their T_g, respectively. This suggested that dodecyl side chains introduced onto bithiophene significantly improved the motion ability of the chain segment. Comparison between the two isoindigo-based polymers revealed PBIBDF-BT with an additional endothermic peak (−33 °C) upon heating and an additional exothermic transition (−37 °C) upon cooling. The latter would be related to melting and crystallization of side chains. The lower side density and more free space in PBIBDF-BT would make its alkyl side chain easier to move.

The molecular conformations of PIID-BT, PIID-BTC12 and PBIBDF-BT were investigated *via* UV-vis-NIR absorption spectroscopy in dilute chloroform solution (Fig. 1e) and thin films cast from the solution (Fig. 1f). PIID-BT showed two distinguishable absorption bands (Fig. 1e). The first absorption band at around 410 nm was associated with the π–π* transition and the second absorption band from 500 to 800 nm was caused by intramolecular charge transfer (ICT), which is typical for donor–acceptor conjugated polymers.[37,38] The maximum absorption peak of PIID-BT polymers in the solution state was recorded at 709 nm. Once two dodecyl side chains were introduced into bithiophene units to form PIID-BTC12, the maximum absorption peak became blue shifted to 601 nm, and the 709 nm absorption peak entirely vanished. This would indicate that additional alkyl side chains could cause large steric hindrance, breaking conjugation in the backbone and weakening the interchain interactions. For BIBDF, the introduction of a lactone group in the central core of isoindigo not only leads to more electron-deficiency but also prolonged its conjugate length. The coexistence of a π–π stacking effect and D–A interaction significantly red-shifted the absorption

spectrum of PBIBDF-BT with a maximum absorption peak recorded at 842 nm. The absorption spectra of all three polymer films exhibited variable degrees of red-shifting when compared to their solution counterparts (Fig. 1f). The latter would suggest improvements in molecular ordering in the solid phase relative to solution due to the strong π–π interchain interactions present in solid thin films.[39] The optical band gaps of PIID-BT, PIID-BTC12 and PBIBDF-BT estimated by the formula (E_g^{opt} = 1240/λ) were 1.47, 1.68 and 1.14 eV, respectively.

The energy levels of these polymer thin films were tested *via* cyclic voltammetry (CV) at a scan rate of 100 mV s^{-1} (Fig. S3, ESI†). The oxidation initiation potential (E_{onset}^{ox}) of PIID-BT, PIID-BTC12 and PBIBDF-BT polymer thin films was recorded as 0.79, 0.85 and 0.86 eV, respectively. The corresponding HOMO levels calculated by the formula (HOMO = $-(E_{onset}^{ox} + 4.75)$) were −5.54, −5.60 and −5.61 eV, respectively. On the other hand, the reduction onset potential (E_{onset}^{red}) values were evaluated to be −1.09, −1.26 and −0.83 eV, respectively. The LUMO energies of PIID-BT, PIID-BTC12 and PBIBDF-BT could be calculated by the formula: LUMO = $-(E_{onset}^{red} + 4.75)$, and were estimated to be −3.66, −3.49 and −3.92 eV, respectively. The corresponding energy band gaps of these films were 1.88, 2.11 and 1.69 eV, respectively (Table 1).

Morphologies of polymer thin films

To gain a better understanding of the crystalline structures and surface morphologies of these polymer thin films, grazing incidence X-ray diffraction (GIXRD) and atomic force microscopy (AFM) were performed and the results are gathered in Fig. 2. According to the 2D GIXRD patterns (Fig. 2a), both PIID-BT and PBIBDF-BT thin films showed distinguishable 4-ordered diffraction peaks of (*h*00) in the out-of-plane q_z direction, suggesting films with highly ordered lamellar structures. Only the (100) diffraction peak was observed for PIID-BTC12 thin films in the out-of-plane q_z direction, indicating a relatively disordered packing structure. For PIID-BT, the (010) diffraction peak appeared only in the in-plane q_{xy} direction, confirming polymer chains with mainly edge-on packing. By contrast, (010) diffraction peaks were observed in both q_z and q_{xy} patterns of PBIBDF-BT, showing mixed face-on and edge-on packing structures. The corresponding lamellar spaces of PIID-BT and PBIBDF-BT thin films were estimated to be 23.35 Å and 25.95 Å, and π–π stacking distances were 3.85 Å and 3.52 Å, respectively. Thus, strong electron-deficient units of BIBDF might improve the polymer backbone planarity and yield smaller π–π stacking distances. The closer π–π stacking distances can be related to higher mobility. For PIID-BTC12, only the (010) diffraction peak was observed in its 2D GIXRD pattern, suggesting PIID-BTC12 thin films have poorly crystalline structures. Long and dense side chains would increase the steric hindrance, resulting in the deterioration of polymer backbone planarity. This, in turn, would affect the molecular packing, leading to poor crystallinity in the thin film state. The atomic force microscopy (AFM) topographies (Fig. 2b) also confirmed PIID-BT with well-organized packing structures, good nanofibrillar surface, and interconnected networks. The latter likely resulted from the strong lamellar stacking. By contrast, no obvious nanofibrillar structures were observed in PIID-BTC12 and PBIBDF-BT thin films. For PIID-BTC12 thin films, the interruption of polymer interchain interactions by the long linear alkyl side chains led to poor crystallinity. Though no obvious nanofibrillar structure was observed on PBIBDF-BT thin film surfaces, they showed the most compact morphologies due to the shorter π–π stacking distances and denser molecular packing.

Mechanical performance of prepared polymer thin films

The mechanical, morphological and electrical properties of the studied polymer thin films were systematically examined under strain. The ductility of polymer thin films can be defined by two specific factors: dichroic ratio and tensile modulus.[4] Elastic moduli can be measured using the buckling method.[40] All films were transferred to a PDMS substrate. When the polymer/PDMS matrix was stretched at 5% strain, periodic buckles appeared due to the mismatch of modulus between the PDMS and polymer thin films. The optical images of thin films deposited on strained PDMS substrates are shown in Fig. 3a.

The elastic moduli of the polymer films could be estimated from their buckling wavelength (λ) using the formula: $\frac{E_f}{1-\nu_f^2} = \frac{3E_s}{1-\nu_s^2}\left(\frac{\lambda}{2\pi d}\right)^3$, where ν_f and ν_s are the Poisson ratios of the conjugate polymer films and the PDMS substrate, respectively. E_f and E_s are the elastic moduli of the conjugate polymer films and the PDMS substrate. λ and d are the periodic buckle wavelength and thickness of the thin films. According to the literature, the elastic moduli of P3HT range between 1000 MPa and 1100 Mpa.[41] Therefore, the P3HT film with similar thickness can be utilized as a standard for data calibration (Fig. S7, ESI†). The tensile moduli of PIID-BT, PIID-BTC12 and PBIBDF-BT were determined to be 784, 102 and 268 Mpa, respectively. The PIID-BT film showed the largest tensile modulus among all three polymer thin films, which might be attributed to its good planarity and high crystallinity. Compared to elastic moduli of conjugated polymers (ranging from 250 Mpa to 800 Mpa),[42] the measured elastic modulus of PIID-BTC12 thin films looked quite small (102 Mpa). This would indicate that introduction of alkyl side chains on

Table 1 Optical and electrochemical properties of the three polymers

Polymer	λ_{max}^{solu} (nm)	λ_{max}^{film} (nm)	λ_{onset}^{film} (nm)	HOMO (eV)	LOMO (eV)	ΔE_g^{CV} (eV)	ΔE_{op} (eV)	M_n/M_w (kg mol^{-1})	PDI
PIID-BT	704	709	845	−5.54	−3.66	1.88	1.47	37/120	3.35
PIID-BTC12	588	601	737	−5.60	−3.49	2.11	1.68	35/94	2.67
PBIBDF-BT	824	842	1084	−5.71	−3.92	1.69	1.14	42/79	1.89

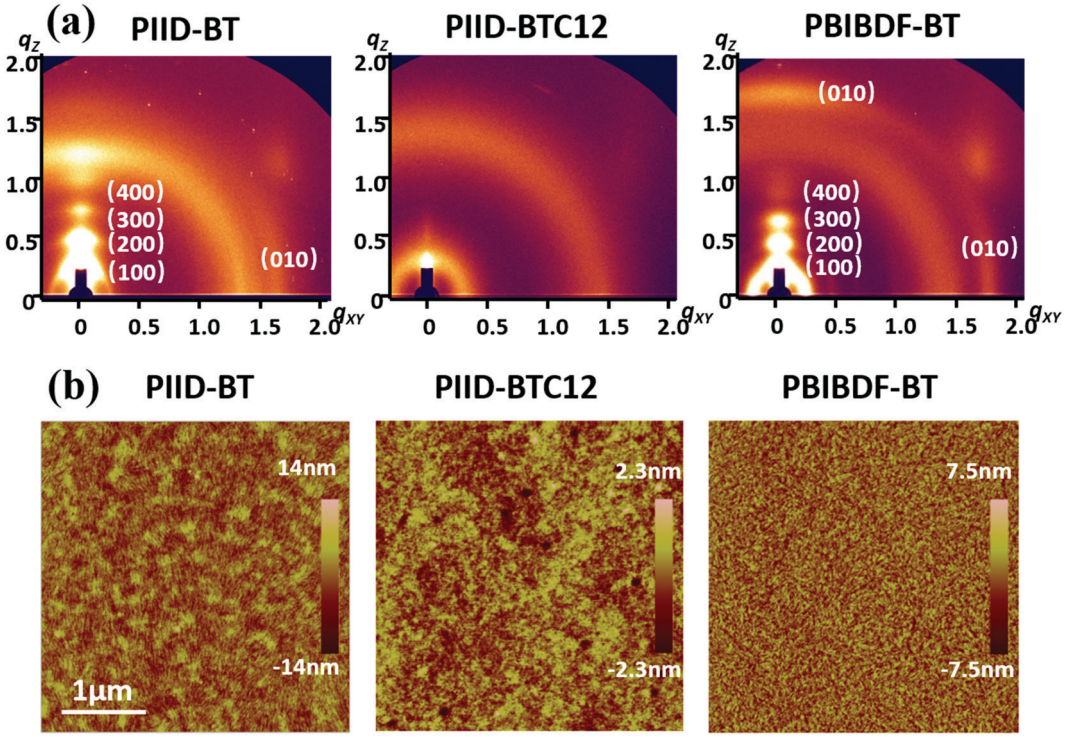

Fig. 2 GIXRD and AFM topographies of PIID-BT, PIID-BTC12, and PBIBDF-BT thin films.

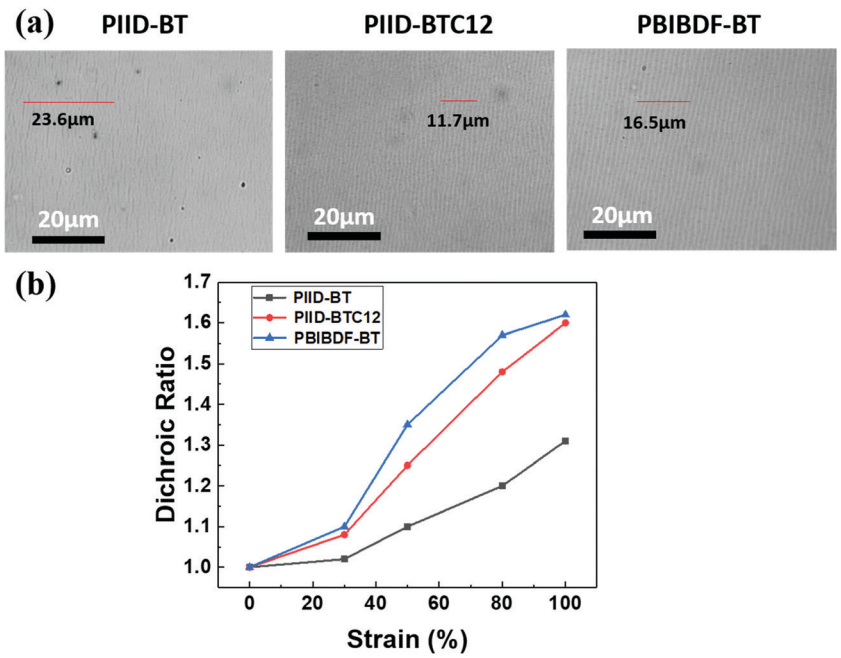

Fig. 3 Optical images of buckled films (a) and the dichroic ratio (R) of the studied polymers under different strain values (b).

thiophene increased the flexibility of molecular chains. Surprisingly, the replacement of IID with BIBDF did not increase the tensile moduli drastically. Although the long conjugate unit doubled the elastic moduli, the PBIBDF-BT thin film moduli are still relatively small when compared to the other conjugated polymers. The dichroic ratio (R) calculated *via* polarized UV-vis spectroscopy is correlated with the degree of polymer chain alignment during stretching (Fig. 3b).[43,44] The R value of PIID-BT thin films gradually increased from 1 to 1.3 as strain changed from 0% to 100%. The R values of PIID-BTC12 and PBIBDF-BT were almost the same at an applied strain of 100% (about 1.6). The higher R value indicated better

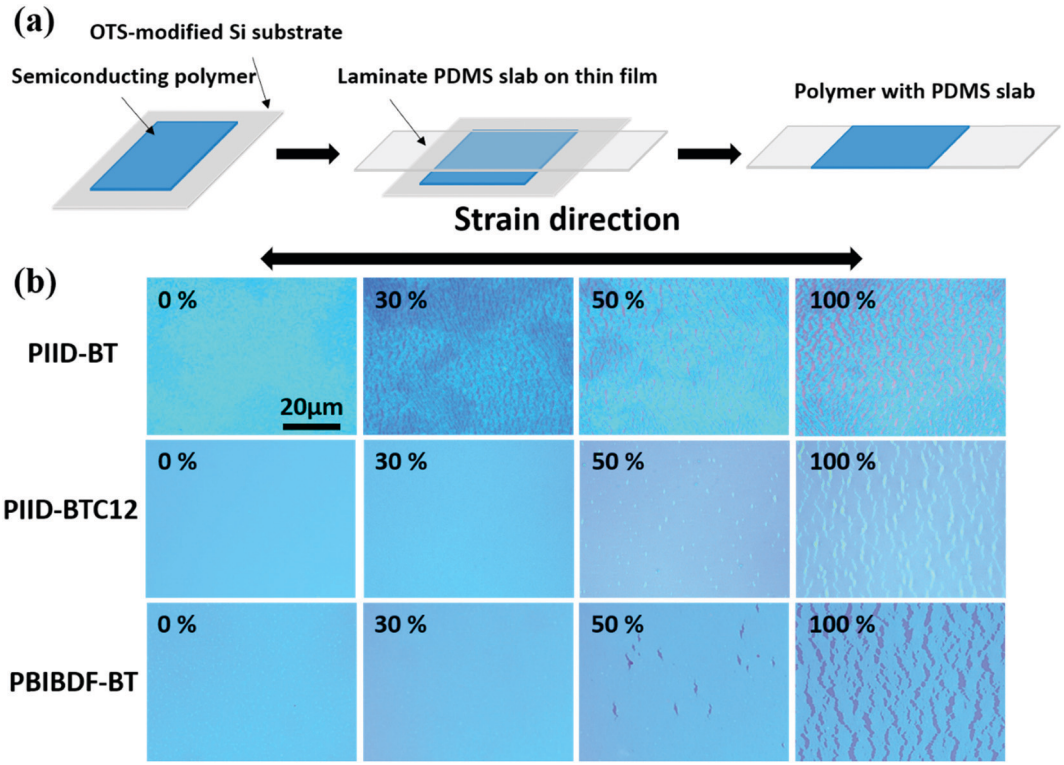

Fig. 4 Preparation process of semiconducting polymer thin films under strain (a). Optical images of thin films under different strains (b).

polymer chain alignment by strain, suggesting the high mechanical tolerance of PIID-BTC12 and PBIBDF-BT thin films when compared to PIID-BT thin films.

The optical microscopy (OM) images (Fig. 4b) clearly showed the differences in mechanical properties among all three polymers thin films. The preparation process of strained polymer thin films is illustrated in Fig. 4a. Numerous cracks clearly formed on PIID-BT thin films under 30% strain (Fig. 4b), consistent with the mechanical properties showing PIID-BT with the largest modulus. No obvious cracks were generated on PIID-BTC12 and PBIBDF-BT thin film surfaces below 50% applied strain. However, the crack width in PBIBDF-BT thin films is much larger than that in PIID-BTC12 thin films when the applied strain approached 100% (Fig. S5, ESI†). Although the long conjugate unit BIBDF induced more brittle thin films of PBIBDF-BT than PIID-BTC12, the long alkyl side chains still ensured good mechanical properties of PBIBDF-BT thin films.

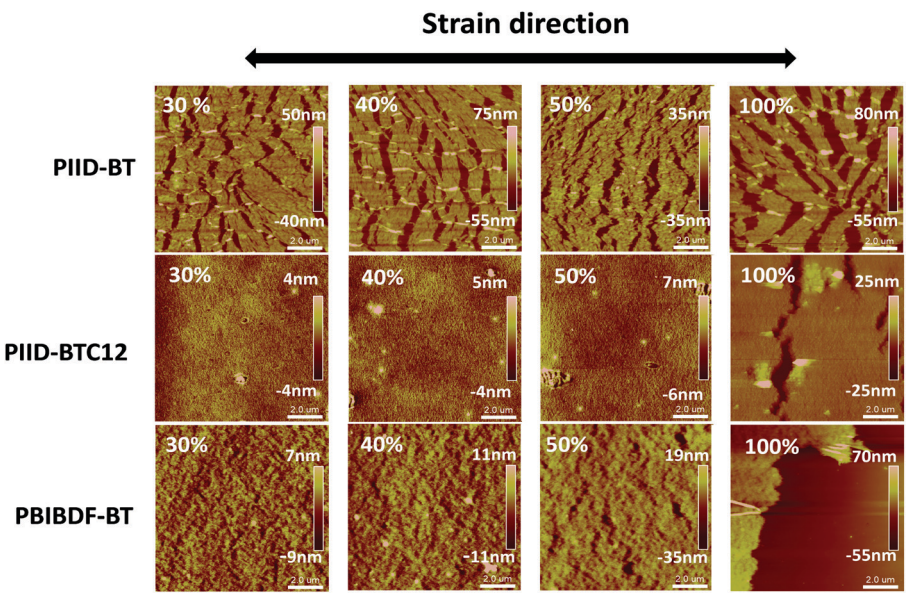

Fig. 5 AFM topographies of stretched thin films.

Similar results were also obtained from AFM topography with higher resolution (Fig. 5). The crack width in PIID-BTC12 thin films was the smallest of all three polymers. The PIID-BTC12 films displayed smooth and flat surfaces even under 40% strain. At strain above 50%, tiny cracks formed on the surface, suggesting that the amorphous region of PIID-BTC12 thin films can induce dissipative external stress. Interestingly, the crack width in PBIBDF-BT thin films was much larger than that in PIID- BT thin films (Fig. S6, ESI†), which could be explained by the mixed packing structure of PBIBDF-BT. The crystallite of the face-on packing plane was parallel to the applied strain, resulting in a much higher influence on the packing structure and formation of larger cracks.[14]

Charge transport characteristics under strain

To evaluate the charge transport behaviors of PIID-BT, PIID-BTC12 and PBIBDF-BT thin films under strain, various OFETs were fabricated and their charge transport properties both parallel and perpendicular to the stretching direction were characterized (Fig. 6a).[45] Unexpectedly, PIID-BTC12 thin films showed no field effect performance in an unannealed state during electrical performance testing. Hence, the mobility value was not calculated here. By comparison, since PBIBDF-BT possessed bipolarity, its P-type and N-type field effect mobilities were calculated separately. In Fig. 6b, both p-type and n-type transfer curves of PBIBDF-BT illustrated very stable transfer characteristics during the stretching process from 0% to 50%

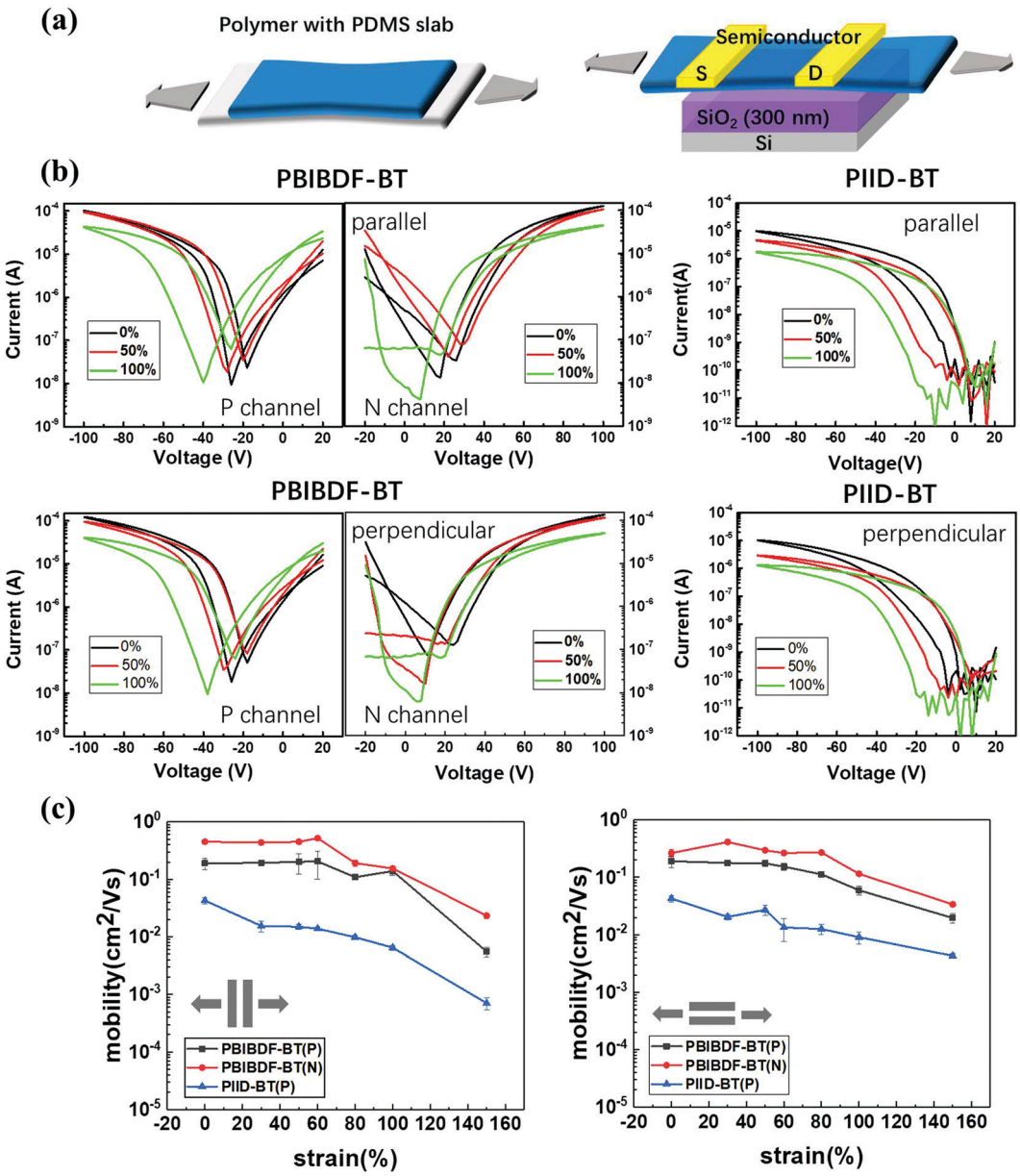

Fig. 6 (a) Fabrication process of a FET device based on the studied semiconducting polymer thin films under strain. (b) Transfer curve of the studied polymer thin films under strain with back and forward sweep. (c) Mobility of the studied polymer thin films under strain.

strain parallel and perpendicular to the stretching direction. Under 100% strain, on-state current decreased slightly and the hysteresis of the curves became large because of the damage of the polymer thin films. For PIID-BT thin films, the on-state current decreased continuously from 0% to 100% strain and the hysteresis increased gradually in both parallel and perpendicular directions. In Fig. 6c, we calculated the mobility of PIID-BT and PBIBDF-BT thin films. PBIBDF-BT exhibited very stable mobility during the stretching process from 0% to 60% strain parallel to the stretching direction. P-type mobility was estimated to be around 0.3 $cm^2\ V^{-1}\ s^{-1}$ and n-type mobility was estimated to be about 0.5 $cm^2\ V^{-1}\ s^{-1}$. An order of magnitude decrease in electrical performance was noticed during stretching from 60% to 150% but still above the order of 10^{-2}. For PIID-BT, the mobility was estimated to be one order of magnitude smaller than that of PBIBDF-BT (about 0.05 $cm^2\ V^{-1}\ s^{-1}$ upon stretching). The mobility declined by an order of magnitude during stretching from 0% to 30%. The downward trend reduced when the film was stretched from 30% to 60%. During stretching from 60% to 150%, the mobility decreased to the order of 10^{-3}. Hence, mobility declined by nearly two orders of magnitude during the whole stretching process. The decrease in mobility correlated well with the formation of cracks.

The decreasing tendency of mobility for both PIID-BT and PBIBDF-BT thin films in the direction perpendicular to that of stretching looked relatively slow when compared to those in the parallel direction. The mobility of PBIBDF-BT did not decline significantly in the strain range of 0% to 60%, while the mobility of PIID-BT slowly decreased at strain exceeding 30%. The changes in on-state current and off-state current on PBIBDF-BT and PIID-BT thin films are provided in Fig. 7. The off-state current substantially maintained a steady state, while the on-state current showed a gradual declining trend, mainly due to a reduced effective charge transfer path caused by mechanical failure. Therefore, the on/off ratio gradually decreased as strain rose.

Table 2 summarizes the maximum mobility and average threshold voltage parallel and perpendicular to the stretching direction from 0% to 150% strain. The maximum mobility of PBIBDF-BT thin films was maintained at the same order of magnitude even when stretched to 100% in both parallel and perpendicular directions to the strain. From 0% to 60% strain, the parallel maximum mobility increased but started declining beyond 80% strain. For PIID-BT thin films, the maximum mobility parallel to the strain direction dropped one order of magnitude at 100% strain. However, the maximum mobility perpendicular to the strain direction maintained the same order of magnitude at 100% strain. The threshold voltages of both polymer thin films were maintained in a relatively stable range. The above morphological and electrical characterization suggested that continuity of strained thin films could be enhanced by incorporating long linear side chains in polymers to lower their tensile moduli in thin film state. Different charge transport properties were also observed as a function of strain. The mobility of PIID-BT thin films declined obviously upon application of the strain. Though PIID-BTC12 and PBIBDF-BT thin films showed similar crack-on-set strains due to their poor packing structures and crystallinities, PIID-BTC12 did not exhibit any field effect properties. By comparison, PBIBDF-BT thin films possessed not only good mechanical properties but also excellent electrical characteristics with relatively low tensile moduli and enhanced packing structures.

The above experimental data revealed that PIID-BT containing branched alkyl side chains with edge-on packing structures

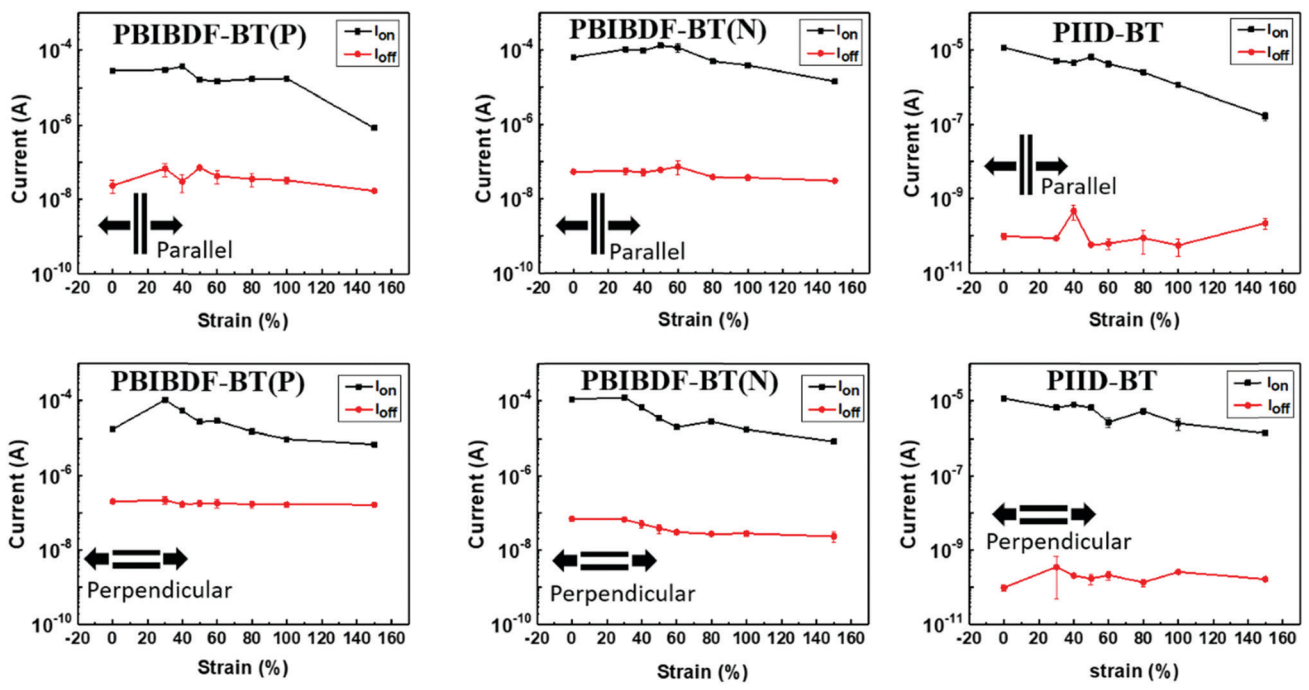

Fig. 7 On and off current of PIID-BT and PBIBDF-BT-based FET devices.

Table 2 Maximum mobility and threshold voltage of PIID-BT and PBIBDF-BT-based FET devices

		PBIBDF-BT(P)		PBIBDF-BT(N)		PIID-BT	
Strain (%)	Direction	μ_{max} ($cm^2\ V^{-1}\ s^{-1}$)	V_{th} (V)	μ_{max} ($cm^2\ V^{-1}\ s^{-1}$)	V_{th} (V)	μ_{max} ($cm^2\ V^{-1}\ s^{-1}$)	V_{th} (V)
0		0.27	−31	0.49	26	0.05	−12
30	Parallel	0.22	−33	0.45	26	0.02	−13
30	Perpendicular	0.21	−26	0.46	29	0.02	−7
40	Parallel	0.30	−31	0.55	25	0.02	−9
40	Perpendicular	0.30	−31	0.46	30	0.03	−8
50	Parallel	0.34	−29	0.48	26	0.02	−12
50	Perpendicular	0.19	−28	0.32	29	0.03	−10
60	Parallel	0.26	−32	0.54	24	0.02	−7
60	Perpendicular	0.18	−30	0.28	24	0.02	−12
80	Parallel	0.12	−30	0.24	24	0.01	−5
80	Perpendicular	0.13	−33	0.30	29	0.02	−12
100	Parallel	0.13	−35	0.17	24	0.01	−5
100	Perpendicular	0.07	−30	0.13	28	0.01	−9
150	Parallel	0.03	−28	0.03	29	0.001	−5
150	Perpendicular	0.03	−33	0.04	26	0.005	−10

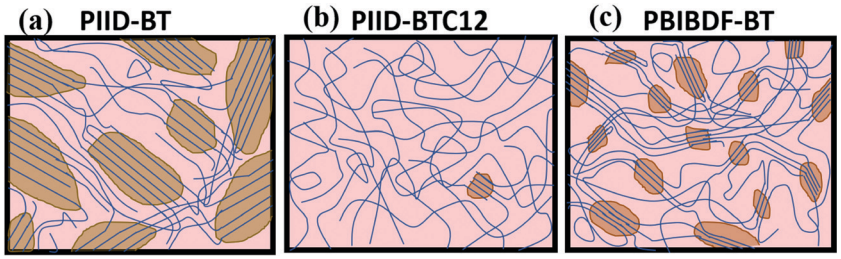

Fig. 8 A schematic representation of the crystallinity of PIID-BT, PIID-BTC12, and PBIBDF-BT.

formed relatively good crystallinity and a high degree of order structure. The DSC data also indicated its rigid backbone structure. A large crystalline region was observed in the AFM topography shown in Fig. 8a. Upon application of strain on PIID-BT thin films, insufficient disordered regions formed and insufficient chain movement occurred to consume the strain inside the thin films. Thus, most applied strain would be consumed by the formation of cracks. This made PIID-BT thin films more brittle among the three polymer thin films. PIID-BTC12 films with C12 alkyl side chains depicted only (100) diffraction peaks in the out-of-plane q_z direction, indicating a significant decrease in crystallization. The latter was also confirmed by AFM, where PIID-BTC12 thin films became chaotic and disordered (Fig. 8b). In this case, strain could be consumed through the disordered region instead of cracks. Overall, the above proposed method significantly improved the ductility of D–A conjugated polymer thin films but inevitably led to a significant drop in field-effect mobility. The addition of a strong electron-deficient long conjugated unit like BIBDF to its acceptor unit yielded a series of distinct diffraction peaks in 2D GIXRD imaging, proposing that addition of BIBDF units significantly improved the molecular packing and crystallinity. The (010) peak in the out-of-plane direction indicated film changes from a simple edge-on packing structure to a new state, with a coexisting edge-on and face-on packing structure. AFM displayed PBIBDF-BT thin films with a small area of crystallization when compared to PIID-BT thin films (Fig. 8c). The DSC data also showed that alkyl side chains significantly improved the chain movement mobility. PBIBDF-BT thin films can maintain similar mechanical resistance as PIID-BTC12 thin films. Moreover, by introducing BIBDF monomers with enhanced local aggregation into the conjugated main chains, the strong intermolecular π–π interaction makes the polymer main chains stack tighter. The smaller π–π stacking distance promoting the charge transfer between molecules and effectively improving the charge transfer ability led to superior mobility over PIID-BT thin films.

4. Conclusion

A series of isoindigo and its derivative based polymers was prepared and characterized to demonstrate how thin film chemical structures influence their mechanical properties. The polymer structures were designed by varying the side chains and backbones to systematically study the intrinsic ductility and mechanical behaviors. The introduction of long linear alkyl side chains lowered the elastic moduli and enlarged the crack-on-set strain, attributed to the formation of a soft amorphous region. But the introduction of long linear alkyl side chains significantly reduced the mobility of thin films because of the decrease of crystallinity. Among both polymers with long linear side chains, BIBDF monomers with enhanced local aggregation in the main chains showed mixed packing structures and small area crystallization. The small π–π stacking distance promoted the charge transfer. The long alkyl side

chains lowered T_g and increased the chain movement ability leading to good mechanical behaviors. The BIBDF polymer thin films exhibited delayed crack propagation at 50% strain with mobility maintained above 0.1 $cm^2 V^{-1} s^{-1}$ at 100% applied strain. Overall, polymers with good electrical and mechanical properties could be obtained by properly adjusting the main and side chains.

Conflicts of interest

There are no conflicts to declare.

Acknowledgements

This study was supported by the National Natural Science Foundation of China (NSFC, 51573036, 51703047), the Distinguished Youth Foundation of Anhui Province (1808085J03), and the Fundamental Research Funds for the Central Universities (JZ2018HGPB0276 and PA2019GDPK0046). The authors thank 9A beamlines (the Pohang Accelerator Laboratory in Korea) for providing the beam time.

References

1 K. Fukuda and T. Someya, *Adv. Mater.*, 2017, 29.
2 M. L. Hammock, A. Chortos, B. C. K. Tee, J. B. H. Tok and Z. Bao, *Adv. Mater.*, 2013, **25**, 5997–6037.
3 T. Kim, J. H. Kim, T. E. Kang, C. Lee, H. Kang, M. Shin, C. Wang, B. W. Ma, U. Jeong, T. S. Kim and B. J. Kim, *Nat. Commun.*, 2015, **6**, 7.
4 S. E. Root, S. Savagatrup, A. D. Printz, D. Rodriquez and D. J. Lipomi, *Chem. Rev.*, 2017, **117**, 6467–6499.
5 S. Savagatrup, A. D. Printz, T. F. O'Connor, A. V. Zaretski and D. J. Lipomi, *Chem. Mat.*, 2014, **26**, 3028–3041.
6 D. J. Lipomi, H. Chong, M. Vosgueritchian, J. Mei and Z. Bao, *Sol. Energy Mater. Sol. Cells*, 2012, **107**, 355–365.
7 B. O'Connor, E. P. Chan, C. Chan, B. R. Conrad, L. J. Richter, R. J. Kline, M. Heeney, I. McCulloch, C. L. Soles and D. M. DeLongchamp, *ACS Nano*, 2010, **4**, 7538–7544.
8 S. Savagatrup, A. S. Makaram, D. J. Burke and D. J. Lipomi, *Adv. Funct. Mater.*, 2014, **24**, 2264.
9 J. A. Rogers, T. Someya and Y. G. Huang, *Science*, 2010, **327**, 1603–1607.
10 T. Sekitani and T. Someya, *Adv. Mater.*, 2010, **22**, 2228–2246.
11 P. Baek, N. Aydemir, Y. An, E. W. C. Chan, A. Sokolova, A. Nelson, J. P. Mata, D. McGillivray, D. Barker and J. Travas Sejdic, *Chem. Mat.*, 2017, **29**, 8850–8858.
12 C. Mueller, S. Goffri, D. W. Breiby, J. W. Andreasen, H. D. Chanzy, R. A. J. Janssen, M. M. Nielsen, C. P. Radano, H. Sirringhaus, P. Smith and N. Stingelin-Stutzmann, *Adv. Funct. Mater.*, 2007, **17**, 2674–2679.
13 J. Xu, S. H. Wang, G. J. N. Wang, C. X. Zhu, S. C. Luo, L. H. Jin, X. D. Gu, S. C. Chen, V. R. Feig, J. W. F. To, S. Rondeau Gagne, J. Park, B. C. Schroeder, C. Lu, J. Y. Oh, Y. M. Wang, Y. H. Kim, H. Yan, R. Sinclair, D. S. Zhou, G. Xue, B. Murmann, C. Linder, W. Cai, J. B. H. Tok, J. W. Chung and Z. N. Bao, *Science*, 2017, **355**, 59–64.
14 C. Lu, W. Y. Lee, X. D. Gu, J. Xu, H. H. Chou, H. P. Yan, Y. C. Chiu, M. Q. He, J. R. Matthews, W. J. Niu, J. B. H. Tok, M. F. Toney, W. C. Chen and Z. N. Bao, *Adv. Electron. Mater.*, 2017, **3**, 13.
15 R. Peng, B. Pang, D. Q. Hu, M. J. Chen, G. B. Zhang, X. H. Wang, H. B. Lu, K. Cho and L. Z. Qiu, *J. Mater. Chem. C*, 2015, **3**, 3599–3606.
16 E. Song, B. Kang, H. H. Choi, D. H. Sin, H. Lee, W. H. Lee and K. Cho, *Adv. Electron. Mater.*, 2016, **2**, 8.
17 S. Goffri, C. Mueller, N. Stingelin-Stutzmann, D. W. Breiby, C. P. Radano, J. W. Andreasen, R. Thompson, R. A. J. Janssen, M. M. Nielsen, P. Smith and H. Sirringhaus, *Nat. Mater.*, 2006, **5**, 950–956.
18 H. F. Wen, H. C. Wu, J. Aimi, C. C. Hung, Y. C. Chiang, C. C. Kuo and W.-C. Chen, *Macromolecules*, 2017, **50**, 4982–4992.
19 H. F. Wen, H. C. Wu, J. Aimi, C. C. Hung, Y. C. Chiang, C. C. Kuo and W.-C. Chen, *Macromolecules*, 2016, **49**, 8540–8548.
20 E. L. Melenbrink, K. M. Hilby, M. A. Alkhadra, S. Samal, D. J. Lipomi and B. C. Thompson, *ACS Appl. Mater. Interfaces*, 2018, **10**, 32426–32434.
21 S. Savagatrup, X. K. Zhao, E. Chan, J. G. Mei and D. J. Lipomi, *Macromol. Rapid Commun.*, 2016, **37**, 1623–1628.
22 J. W. Mun, G. J. N. Wang, J. Y. Oh, T. Katsumata, F. L. Lee, J. Kang, H. C. Wu, F. Lissel, S. Rondeau Gagne, J. B. H. Tok and Z. N. Bao, *Adv. Funct. Mater.*, 2018, **28**, 10.
23 Y. J. Jin, J. E. Bae, K. S. Cho, W. E. Lee, D. Y. Hwang and G. Kwak, *Adv. Funct. Mater.*, 2014, **24**, 1928–1937.
24 G. J. N. Wang, L. Shaw, J. Xu, T. Kurosawa, B. C. Schroeder, J. Y. Oh, S. J. Benight and Z. N. Bao, *Adv. Funct. Mater.*, 2016, **26**, 7254–7262.
25 H. J. Kim, J.-H. Kim, J.-H. Ryu, Y. Kim, H. Kang, W. B. Lee, T.-S. Kim and B. J. Kim, *ACS Nano*, 2014, **8**, 10461–10470.
26 R. Kroon, D. Kiefer, D. Stegerer, L. Yu, M. Sommer and C. Mueller, *Adv. Mater.*, 2017, 29.
27 T. Lei, Y. Cao, Y. Fan, C. J. Liu, S. C. Yuan and J. Pei, *J. Am. Chem. Soc.*, 2011, **133**, 6099–6101.
28 T. Lei, J. H. Dou, Z. J. Ma, C. H. Yao, C. J. Liu, J. Y. Wang and J. Pei, *J. Am. Chem. Soc.*, 2012, **134**, 20025–20028.
29 J. Mei, H. C. Wu, Y. Diao, A. Appleton, H. Wang, Y. Zhou, W. Y. Lee, T. Kurosawa, W. C. Chen and Z. Bao, *Adv. Funct. Mater.*, 2015, **25**, 3455–3462.
30 H. C. Wu, C. W. Hong and W. C. Chen, *Polym. Chem.*, 2016, **7**, 4378–4392.
31 Y. Q. Zheng, Z. Wang, J. H. Dou, S. D. Zhang, X. Y. Luo, Z. F. Yao, J.-Y. Wang and J. Pei, *Macromolecules*, 2015, **48**, 5570–5577.
32 G. Zhang, Y. Fu, Z. Xie and Q. Zhang, *Macromolecules*, 2011, **44**, 1414–1420.
33 G. Zhang, P. Li, L. Tang, J. Ma, X. Wang, H. Lu, B. Kang, K. Cho and L. Qiu, *Chem. Commun.*, 2014, **50**(24), 3180–3183.
34 Z. Yan, B. Sun and Y. Li, *Chem. Commun.*, 2013, **49**, 3790–3792.
35 Y. Ito, A. A. Virkar, S. Mannsfeld, J. H. Oh, M. Toney, J. Locklin and Z. Bao, *J. Am. Chem. Soc.*, 2009, **131**, 9396–9404.

36 D. Rodriquez, J.-H. Kim, S. E. Root, Z. Fe, P. Boufflet, M. Heeney, T. S. Kim and D. J. Lipomi, *ACS Appl. Mater. Interfaces*, 2017, **9**, 8855–8862.
37 T. Lei, J. H. Dou and J. Pei, *Adv. Mater.*, 2012, **24**, 6457–6461.
38 G. Zhang, P. Li, L. Tang, J. Ma, X. Wang, H. Lu, B. Kang, K. Cho and L. Qiu, *Chem. Commun.*, 2014, **50**, 3180–3183.
39 X. Zhao, D. Yang, H. Lv, L. Yin and X. Yang, *Polym. Chem.*, 2013, **4**, 57–60.
40 D. Tahk, H. H. Lee and D. Y. Khang, *Macromolecules*, 2009, **42**, 7079–7083.
41 S. Savagatrup, A. D. Printz, T. F. O'Connor, A. V. Zaretski, D. Rodriquez, E. J. Sawyer, K. M. Rajan, R. I. Acosta, S. E. Root and D. J. Lipomi, *Energy Environ. Sci.*, 2015, **8**, 55–80.
42 B. Roth, S. Savagatrup, N. V. de los Santos, O. Hagemann, J. E. Carlé, M. Helgesen, F. Livi, E. Bundgaard, R. R. Søndergaard, F. C. Krebs and D. J. Lipomi, *Chem. Mater.*, 2016, **28**, 2363–2373.
43 J. Y. Oh, S. Rondeau-Gagne, Y. C. Chiu, A. Chortos, F. Lissel, G. J. N. Wang, B. C. Schroeder, T. Kurosawa, J. Lopez, T. Katsumata, J. Xu, C. Zhu, X. Gu, W. G. Bae, Y. Kim, L. Jin, J. W. Chung, J. B. H. Tok and Z. Bao, *Nature*, 2016, **539**, 411–415.
44 J. T. Wang, S. Takshima, H. C. Wu, C. C. Shih, T. Isono, T. Kakuchi, T. Satoh and W. C. Chen, *Macromolecules*, 2017, **50**, 1442–1452.
45 B. O'Connor, R. J. Kline, B. R. Conrad, L. J. Richter, D. Gundlach, M. F. Toney and D. M. DeLongchamp, *Adv. Funct. Mater.*, 2011, **21**, 3697–3705.